Materials Research Proceedings 41 (2024) 1150-1158 https://doi.org/10.21741/9781644903131-127

The experimental full-field method (EFFM) for parameter calibration applied on an anisotropic constitutive model

ILG Christian[1,a*], SHETTY Mayank[1,b], KARADOGAN Celalettin[1,c], HAUFE André[1,d] and LIEWALD Mathias[2,e]

[1]DYNAmore an ANSYS Company, Industriestraße 2, 70565 Stuttgart, Germany

[2]Institute for Metal Forming Technology (IFU), Holzgartenstraße 17, 70174 Stuttgart, Germany

[a]christian.ilg@ansys.com, [b]mayank.shetty@ansys.com, [c]celal.karadogan@ansys.com, [d]andre.haufe@ansys.com, [e]mathias.liewald@ifu.uni-stuttgart.de

Keywords: FEA, Parameter Identification, DIC, Optimization

Abstract. Accurate characterization of material models is essential to ensure a higher prediction quality in Finite Element Analysis (FEA) under general loading conditions in sheet metal forming. Achieving accurate material model data frequently involves intricate inverse analysis techniques and numerous experimental tests. To overcome the complexities associated with calibration processes, the adoption of optical measuring systems like Digital Image Correlation (DIC) is widespread in material model calibration. The rich information obtained from DIC measurements is often used by material model calibration strategies to calibrate the values of material or model parameters, such as extrapolation of stress-strain curves or Lankford parameters that are not necessarily constant over the entire range of plastic deformation. This study presents the Experimental Full-Field Method (EFFM) as an innovative iterative approach for the calibration of material properties. As a special implementation of Finite Element Model Update (FEMU) [1], the EFFM uses the whole deformation field gained from DIC as boundary conditions [2]. This is then used in an inverse optimization procedure to determine parameters of complex material models. In this research, the EFFM is applied to an anisotropic constitutive model [3] to optimize three flow curves in 0°, 45° and 90° directions w.r.t. the rolling direction and the yield surface exponent, which reflects the polycrystal structure of the sheet material, to define the shape of the evolving yield locus in stress space. This is achieved by a modified tensile test specimen with L-shaped cut-outs which allows a distribution of higher strain values over a wider range of triaxiality values. With the direct use of the experimental deformation field in the FE simulation, displacements and strains are not any more objects of the optimization but only stresses. This also eliminates the step of mapping between experiments and simulations. Moreover, by using implicit time integration the inversion of the stiffness matrix becomes redundant, as positions of all nodes are already predetermined at each time step. These aspects make EFFM faster and more accurate than conventional FEMU.

Background

Accurate representation of material behavior within FEA is a cornerstone for predicting the structural response of components and systems under various loading conditions. The fidelity of FEA predictions directly hinges on the precision of the material models employed. These models encapsulate the intricate relationships between applied forces, deformation, and the resulting stress and strain distributions within a material.

However, characterizing material behavior for FEA purposes is a complex task laden with challenges. Materials often exhibit nonlinear, anisotropic, and time-dependent behaviors under various loading conditions. Traditional approaches to material characterization often rely on simplistic models or standardized test data, which may inadequately capture the nuanced behavior

of materials in real-world applications. This discrepancy between actual material behavior and model representation poses a significant challenge in achieving accurate FEA predictions.

This is where Optical Measuring Systems, particularly DIC, have emerged as invaluable tools in material model calibration. DIC systems enable high-resolution, full-field measurements of surface deformation on materials subjected to loading. They provide detailed information about the displacement and strain fields across the material's surface, offering a wealth of data for characterizing material behavior. This detailed deformation information, when integrated within FEA, allows for a more accurate calibration of material models. Avril et al. [4] wrote a valuable review on parameter identification methods.

Introduction of the EFFM

Utilizing a DIC system (12 mega pixels GOM ARAMIS system) the complete displacement field of a specimen can be acquired, exported as XML-file, and transformed into boundary conditions using the Envyo® mapping software. These imposed boundary conditions are then applied to all nodes within the corresponding LS-DYNA® simulation model, resulting in the creation of a digital replica (digital twin) of the specimen's geometry and experimental kinematics.

Using the digital twin as a basis, an iterative optimization process in LS-OPT® can be initiated to calibrate miscellaneous parameters of all material models available in LS-DYNA across various materials. Global force-time curves integrated over many hypothetical cross sections over the specimen or local force equilibriums at different nodes can be employed as objective functions for the optimization process. Prior to this, one must be aware of the experimental data or digital twin that should be used for the calibration of a specific material or parameters in a material model.

Utilizing experimental displacements directly obviates the necessity of employing displacements or strains as the optimization target. The optimization is based on stresses that are calculated from inherited strains. A significant advantage of directly feeding the measured displacements as boundary conditions in simulations, as opposed to classical FEMU, is the enhanced speed of conducting simulations. When calculating a digital twin with implicit time integration, the inversion of the stiffness matrix becomes unnecessary, as node positions are already predetermined at each time step.

Application of the EFFM

The following chapter explores the application of the EFFM using the sheet metal DP800 and the calibration of its material parameters as an example and its calibration for an anisotropic material model as an example. The application of the EFFM is partly derived from prior works that have influenced aspects such as data filtering, the selection of the material model, and the shape of the specimen geometry [2]. The thickness of the DP800 sheet is 1.5 mm, and the specimens used were obtained through waterjet cutting at 0°, 45°, and 90° angles relative to the rolling direction of the steel sheet. The specimens were subsequently printed using a UV LED printer to ensure a high-quality speckle pattern across the entire specimen. This helps to avoid reflections and DIC errors caused by unsuitable patterns. Finally, the specimens are tested using a universal tensile testing machine.

*Material model***.** Prior experiments employing the specified methodology based on the experimental deformation field have demonstrated that optimizing basic material models, such as the von Mises yield criterion (*MAT_024 in LS-DYNA) [5], yields unsatisfactory outcomes. Even standard tensile specimen geometries with a rectangular gauge shape manifest intricate material behaviors, for example in the localization zone, which cannot be realistically replicated using basic material models.

Consequently, an orthotropic plasticity model, specifically the material model denoted as *MAT_036E in LS-DYNA [5], was chosen for this study. This model is created based on the

framework proposed by Barlat and Lian in 1989 [6]. To enhance its versatility, the model was extended to accommodate distinct strain hardening curves applicable to the three in-plane rolling directions (0°, 45°, and 90°), as well as for shear and equibiaxial tension. Whereby the flow curves in shear and equibiaxial tension are not obligatory. Additionally, the HOSF=1 option was employed, mitigating the presence of a concave yield locus. This is achieved by utilizing solely the information pertaining to anisotropy in the flow curves and incorporating Lankford parameters exclusively for the plastic flow rule, as detailed in the paper by Andrade et al. [3]. Therefore, if the principal and material axes are coincident, the yield locus can be described as

$$\Phi(\boldsymbol{\sigma}) = \frac{1}{2}(|\sigma_1|^m + |\sigma_2|^m + |\sigma_1 - \sigma_2|^m) - \sigma_y^m\left(\sigma_y^0, \sigma_y^{45}, \sigma_y^{90}, \sigma_y^s, \sigma_y^b\right) = 0. \quad (1)$$

The exponent *m* in Eq. 1 determines the curvature near points of deviatoric uniaxial tensile and compressive stress and represents the polycrystal structure of the sheet material.

In the material card calibration carried out in this work, the exponent of the yield surface and three parameterized flow curves are optimized for the different extraction angles relative to the rolling direction. The initial estimation of the flow curve is based on experimental tensile tests and the conversion of the extracted engineering stress strain curves [7]. Retaining the experimental yield stresses up to the point of diffuse necking and ensuring *C1*-continuity thereafter, the Hockett-Sherby hardening law [8] is employed to calculate the subsequent yield stress values:

$$\sigma_y\left(\varepsilon_{pl}\right) = A - Be^{(-c\varepsilon_{pl}^n)}. \quad (2)$$

In the Hockett-Sherby equation, due to the C1-continuity condition, the parameters *A* and *B* are excluded from the variable parameter list of the optimization and only the *c* and *n* are used as variables to be optimized.

Specimen geometry. In order to obtain as much data as possible for the calibration of an anisotropic material model while minimizing the number of experiments, novel specimen geometries can be employed [9,10]. Ilg et al. [11] introduced an innovative method for optimizing tensile specimen geometries, based on the distribution of plastic strains over stress triaxiality. This approach ensures coverage of all possible loading scenarios by the specimen geometry, with the ability to selectively emphasize or neglect specific regions in the diagram.

During the computational optimization of such a specimen geometry using the aforementioned methodology, several considerations must be taken into account: Firstly, the simulation must already possess high predictive accuracy. This implies that the material model used for specimen geometry optimization should already be characterized to a certain accuracy based on the experimental data. Additionally, when optimizing with shell elements, it is crucial to use at least three integration points across the shell thickness to accurately capture twisting/warping of the tensile specimen during virtual load application. Furthermore, attention should be given to the manufacturability of the specimen, avoiding small cutouts, angles, or radii. Such extreme shapes can distort the optimization results, as very short sides may cause irregular elements with poor aspect ratio may need to be fitted in these areas, leading to unphysical stress states or extremely high strains.

Another important factor for the optimization is the vertical symmetry of the tensile specimen. Testing vertically asymmetric tensile specimens results in transversal displacements at clamping jaws during testing, leading also to transversal forces that most load cells cannot measure. If the optimization target of the material calibration involves the global force, only vertically symmetric tensile specimens should be used.

For this reason, the specimen geometry with L-shaped holes used in a previous work [2] was modified to achieve vertical symmetry. Fig. 1 illustrates the technical drawing of the specimen geometry used in this study.

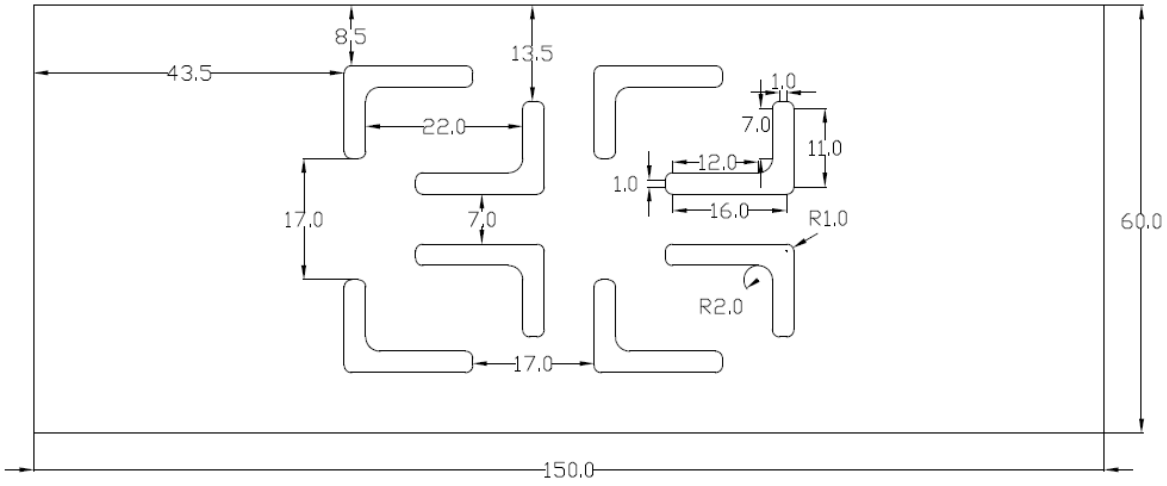

Fig. 1. Technical drawing of the specimen geometry with 8-L-shaped cut-outs and vertical symmetry.

The tensile specimen with vertical symmetry does not achieve the wide-ranging distribution of stress triaxiality exhibited by the asymmetric specimen; however, it still demonstrates a superior distribution compared to conventional tensile specimen geometries. Fig. 2 displays the traces of load paths of the elements in stress space (left) and the plastic strain over stress triaxiality (right) just before the deletion of the first shell element. These diagrams not only capture a snapshot just prior the simulations terminate but also include the history of load paths.

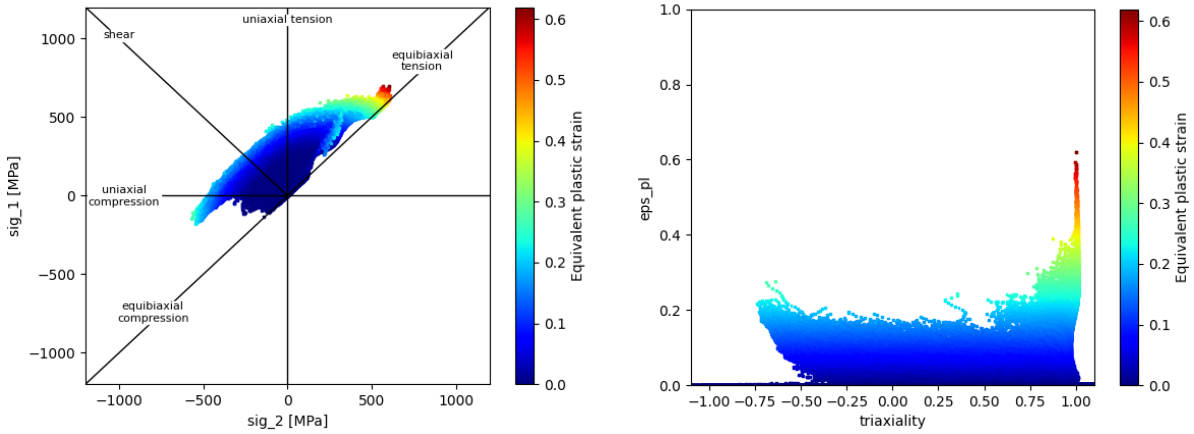

Fig. 2. Distribution of the equivalent plastic strain in the principal stress space (left) and via stress triaxiality (right).

Fig. 3 exemplifies displacement-time curves for various facet mid-points respectively nodal points within different loading zones. The digital twin, presented in the upper left corner of the diagram, illustrates the regions from which the node information for the curves was extracted. The green region lies directly at the upper clamping device within the force initiation zone, the orange

region is situated in the middle of the tensile specimen, and the blue region is near the lower clamping device.

The displacements of all facet mid-points only in the vertical and horizontal directions were converted into boundary conditions for the simulation, with no consideration given to displacements in the thickness direction.

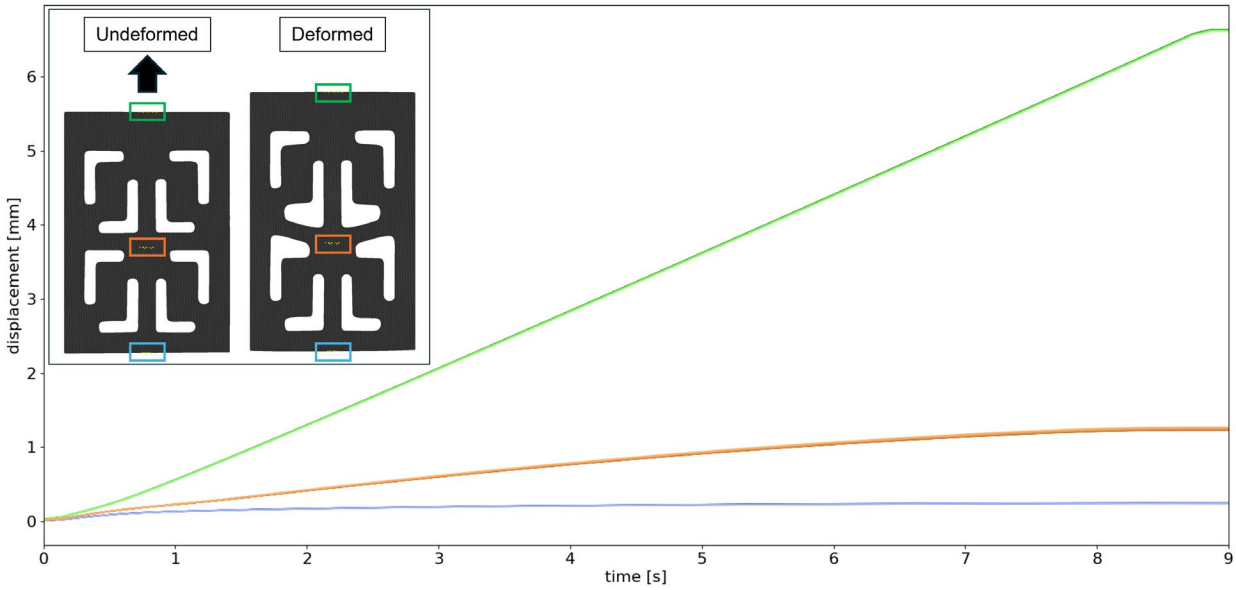

Fig. 3. Displacement-time curves of various nodal points in different load areas and the digital twin, undeformed and deformed, in the top left corner.

Definition of optimization targets. Based on the digital twin, an iterative optimization process can now be initiated. In this study, two optimization criteria were applied to assess their utility in this methodology. On the one hand, a force-time criterion, further termed “Global Force”, was employed, wherein the global force is integrated using three different cross sections through the specimen and calibrated to match the experimentally measured global force. A drawback of this criterion is the loss of information at the edge of the specimen by the optical measurement system, necessitating compensation through scaling of the simulated force-time curves. The locations of the hypothetical sections in the digital twin are depicted in Fig. 4, positioned in the lower, middle, and upper regions of the specimen.

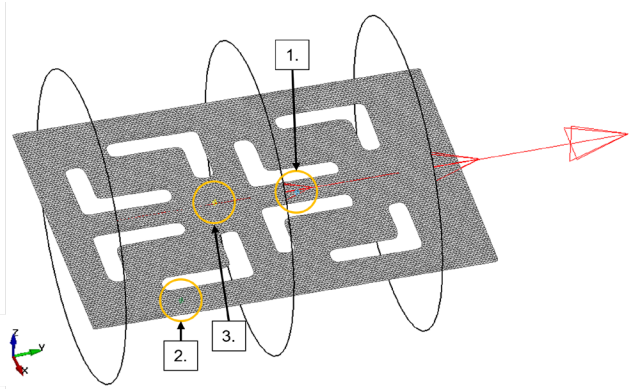

Fig. 4. Visualization of the three cross sections (black circles) and the nodes highlighted with orange circles which are used for the different methodologies.

On the other hand, a criterion based on the force equilibrium at nodes, further termed “Split Nodes”, is applied. Individual nodes are split, and their direction-dependent forces are summed. The resulting force of these nodes must be equal to zero. In Fig. 4, three positions where this criterion was applied are marked with orange circles. When selecting nodes, it is crucial to ensure they are in regions of high plastic strains, at least above the uniform strain, as the flow curve is partially predefined and only extrapolated part is fitted, as outlined in Eq. 2. A schematic drawing illustrating the node splitting process for a single nodal point is presented in Fig. 5. Activating the option to split nodes of the digital twin can be activated in the Envyo mapping software.

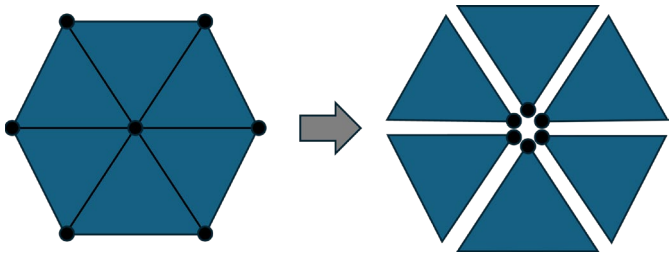

Fig. 5. Schematic illustration of the splitting nodes option for a single nodal point.

Results of the EFFM

In this section, the results of the optimization using the chosen strategies, "Global Force" and "Split Nodes," are revealed. The optimization results using the "Global Force" method are depicted in Fig. 6. The lines marked with crosses represent the global force-time curves from the experimental tests at 0°, 45°, and 90° to the rolling direction. The solid curves illustrate the integrated force from the middle cross-section of each simulation. The blue curves represent the force-time curves of the baseline run, which does not involve parameter optimization, and the red curves represent the force-time curves after 15 iterations.

The results indicate no significant improvement after the parameter optimization. The deviations from the experimental force-time curves only marginally decrease compared to the first iteration. The reason for this lies in the selection of the locations of the cross sections in the digital twin. The regions traversed by these cuts exhibit no plastic strains exceeding the uniform elongation strain. This implies that there is no information in the cuts necessary for flow curve extrapolation.

Furthermore, it is noteworthy that the force curves are highly noisy. Despite filtering the experimental data and the seemingly smooth displacement-time curves of individual facet mid-points, noise-free curves cannot be obtained in the simulation.

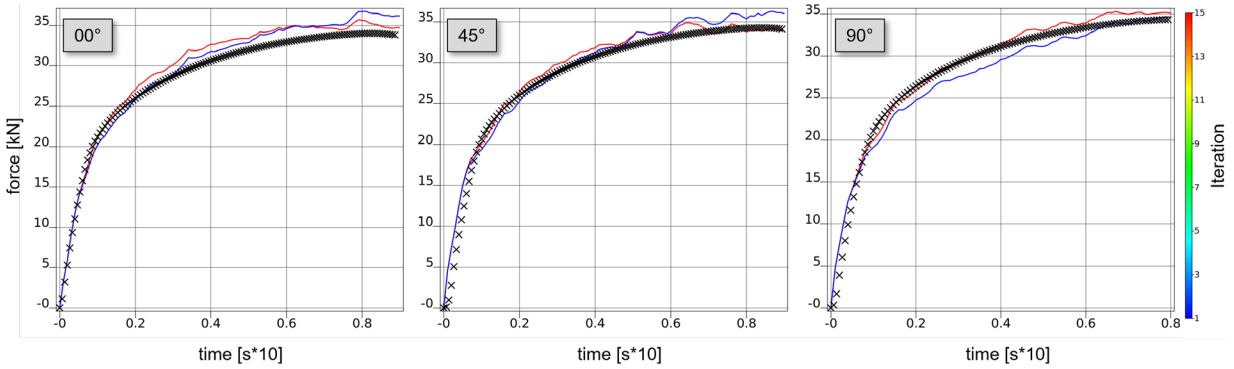

Fig. 6. Optimization results showing the global force-time curves from the experimental tests at 0°, 45°, and 90° to the rolling direction.

The results of the optimization using the "Split Nodes" method are presented in Fig 7. The diagram illustrates the resulting force-time curves in loading and transversal direction, exemplified at the first node (Fig. 4), of the digital twin extracted in the rolling direction. The blue curves represent the resulting force-time curves of the baseline run, which does not involve parameter optimization, and the red curves represent the resulting force-time curves after 15 iterations. The results show a substantial improvement in the force equilibrium after the parameter optimization. However, a complete force equilibrium could not be achieved.

Upon examining the curve plots, it is noticeable that the noisy measurement data is also reflected in noisy simulation data.

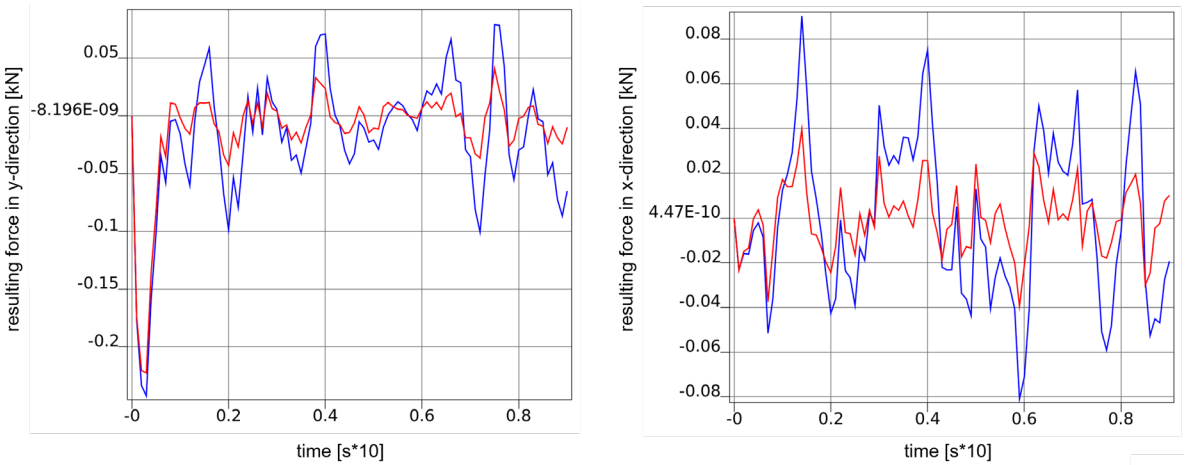

Fig. 7. Optimization results showing the force equilibrium over time in loading direction (left) and in transversal direction (right).

Summary

In the present study, a parameter-identification procedure called EFFM was carried out for the calibration of an anisotropic material model. Containing the calibration of three flow curves extrapolated according to a modified Hockett-Sherby approach and the exponent of the yield surface based on the optical full-field measurement. Within the EFFM one is able to build a digital twin by using local displacement measurements during the test and using this information as boundary conditions for a corresponding FE mesh.

For the method a modified L-shaped specimen geometry was used to enable more accurate and representative measurements of the strain field under complex loading conditions, including uniaxial tension, plane strain, and equibiaxial tension.

The optimization of the variables used in the modified Hockett-Sherby extrapolation approach and the exponent of the yield surface based on the new tensile test specimen and with the global force as an optimization target shows a poor agreement regarding the experiment. The results obtained can be attributed to multiple factors: Noise in the experimental measurement data, the conversion of the experimental data and inadequate spatial discretization. Noise in experimental measurement data, if not correctly accounted for, may also lead to inaccurate simulation results. Furthermore, a deviation already occurs when converting the optical measurement data into a simulation model, as the optical measurement is performed on the sample surface and projected into the shell mid-plane. Additionally, the chosen shell formulation for spatial discretization was not capable of capturing stress in the thickness direction, which may result as well in inaccurate simulation results w.r.t. three-dimensional stress states developing in necking and localization regions.

The optimization based on a criterion with split nodes shows a more satisfactory result. But the noise in the measurement data is as well visible in the resulting simulative force-time curves. This underscores the importance of data quality and preprocessing of the optical measurement data.

There are further factors that influence the results of both methods: the exclusion of displacements in the thickness direction and the absence of strain rate effects in the material model that was used. To improve the accuracy of the method, a conversion which results in boundary conditions on the shell surface, with displacements in thickness direction should be implemented, DIC data smoothing and filtering techniques in space and time to fight the noise in the measurement data, and alternative shell formulations or the use of multiple solid elements across the sheet metal thickness should be considered. To investigate the effect of noise, still images can be used to understand the ground noise and eliminate it before using the displacement field with the Envyo mapping software. Clearly, both of which require further assumptions about the section deformation through the thickness direction. Hence, an improved approach, with careful enhancements of the experimental data in lateral direction, could be to map the deformation field onto a regular, very fine 3D mesh as already proposed by Liebold et al. [12]. Furthermore, optimization criteria that include the vanishing of stress divergence at multiple or even all nodes can be tested [13].

The method is also promising when it is coupled with Digital Volume Correlation (DVC) for materials which allow full 3D computerized tomography (CT) to capture internal displacement fields.

Acknowledgments

The authors would like to thank Stefan Wacker, Christian Liebold and Dr. Nils Karajan for performing the experiments at the laboratory of the Material Competence Center in Stuttgart, Germany, for code development and for their advice. Their help and support are greatly acknowledged.

This work has been carried out within the research project AIMM (Artifical Intelligence for Material Models) funded by the Federal Ministry for Economic Affairs and Climate Action (BMWK) under the grant number 19 | 20024A.

References

[1] R. Mahnken, E. Stein, A unified approach for parameter identification of inelastic material models in the frame of the finite element method, J. Computer Methods in Applied Mechanics and Engineering 136, 1996, pp. 225-258. https://doi.org/10.1016/0045-7825(96)00991-7

[2] C. Ilg, C. Liebold, A. Haufe, V. Sreenivasa, C. Karadogan, M. Liewald, Displacement driven simulation and material calibration based on digital image correlation Part II – Application, IOP Conf. Ser.: Mater. Sci. Eng. 1284, 2023. https://doi.org/10.1088/1757-899X/1284/1/012056

[3] F. Andrade, T. Borrvall, P. DuBois, M. Feucht, A Hosford-based orthotropic plasticity model in LS-DYNA, 12th European LS-DYNA Users' Conference, 2019

[4] S. Avril, M. Bonnet, A.-S. Bretelle, M. Grèdiac, F. Hild, P. Ienny, F. Latourte, D. Lemosse, S. Pagano, E. Pagnacco, F. Pierron, Overview of identification methods of mechanical parameters based on full-field measurements, Experimental Mechanics 48, 2008, pp. 381–402. https://doi.org/10.1007/s11340-008-9148-y

[5] Livermore Software Technology 2020 LS-DYNA Keyword User's Manual vol 2 R12

[6] F. Barlat, K. Lian, Plastic behavior and stretchability of sheet metals. Part I: A yield function for orthotropic sheets under plane stress conditions, Int. J. Plasticity 5, 1989, pp. 51-56. https://doi.org/10.1016/0749-6419(89)90019-3

[7] C. Ilg, A. Haufe, K. Witowski, D. Koch, M. Liewald, Parameter identification using full-field calibration (FFC), IOP Conf. Ser.: Mater. Sci. Eng. 651, 2019, doi:10.1088/1757-899X/651/1/012070

[8] J.E. Hockett, O.D. Sherby, Large strain deformation of polycrystalline metals at low homologous temperatures, J. of the Mech. and Phys. of Solids 23, 1975, pp. 87-98. https://doi.org/10.1016/0022-5096(75)90018-6

[9] M. Gonçalves, M. G. Oliveira, S. Thuillier, A. Andrade-Campos, On the comparison of heterogeneous mechanical tests for sheet metal characterization, Materials Research Proc. 28, 2023, pp. 1121-1130. https://doi.org/10.21741/9781644902479-123

[10] B. Williams, C. Simha, On the design of novel multi-failure specimens for ductile failure testing, IOP Conf. Ser.: Mater. Sci. Eng. 651, 2019, https://doi.org/10.1088/1757-899X/651/1/012091

[11] C. Ilg, A. Haufe, V. Sreenivasa, C. Karadogan, M. Liewald, Parameter identification applying full-field calibration (FFC) techniques, Proc. of the 14th Int. Conf. on the Techn. of Plast., 2023, pp. 578-585. https://doi.org/10.1007/978-3-031-42093-1_55

[12] C. Liebold, C. Ilg, A. Haufe, T. Usta, V. Sreenivasa, Displacement based simulation and material calibration based on digital image correlation Part I – Theory, IOP Conf. Ser.: Mater. Sci. Eng. 1284, 2023, https://doi.org/10.1088/1757-899X/1284/1/012053

[13] P. Böhringer, D. Sommer, T. Haase, M. Barteczko, J. Sprave, M. Stoll, C. Karadogan, D. Koch, P. Middendorf, M. Liewald, A strategy to train machine learning material models for finite element simulations on data acquirable from physical experiments, Comp. Meth. in Applied Mech. and Eng. 406, 2023, https://doi.org/10.1016/j.cma.2023.115894